Tests and simulations of GEM foils for use in an active target gaseous detector

M. Sc. Thesis

Author:
Jacob Snäll

Supervisor:
Joakim Cederkäll

February 1, 2016

Lund University

Abstract

The HIE-ISOLDE post accelerator at CERN has recently come online, enabling the use of radioactive ion beams with energies of up to 10 MeV/u. An active target gaseous detector is under development for use in some of the experiments. The first investigation of the electron amplification stage with gas electron multipliers has been performed. To this end, a small prototype GEM detector was built and tested. The results from these tests are compared with simulations done with the package Garfield++. The gain was measured for three different gas mixtures of Ar/CO_2 in the ratios 70/30, 76/24, and 82/18. The gain for these cases were ca 1500, 4500, and 15000. The simulations of the gain for the same gas mixtures gave the result 1100, 3000, and 9500. The measurements and the simulations show good agreement, but worse with less quencher in the gas mixture. A charge up test of the detector was performed resulting in a charge up time of roughly five hours and a relative gain increase of 1.6. The spread of the electron cloud at the readout plane was simulated and was in the order of $\sim$1 mm. Practical handling routines for changing of GEM foils in the detector in a clean room were also developed.

Acknowledgment

I would like to thank my supervisor Joakim Cederkäll for continuous help, support and discussions. A special thanks goes to Eraldo and the helpful people at CERN, for advice on the handling and testing of the GEM foils. Finally a thanks to Håkan and George at Lund Nano Lab for help with access to the clean room.

Contents

List of Figures

Chapter 1

Introduction

1.1 Background

This work investigates the electron amplification stage of a detector for reactions with radioactive ion beams intended to be used at ISOLDE at CERN. ISOLDE provides radioactive ion beams for nuclear physics experiments using the Isotope Separator On-line (ISOL) technique. A proton beam with an energy of 1.4 GeV and a repetition rate of $\sim$1 Hz is extracted from the PS-booster, which is one of the pre-acceleration stages for the LHC. The beam hits a thick target and creates different isotopes by spallation and fission. The desired isotope is ionized, e.g. by tuned lasers, cooled and bunched before being post-accelerated for use in experiments. In a new development the HIE-ISOLDE post accelerator has recently come online. It enables further acceleration of the ion beams to energies up to 10 MeV/u. The higher energies enable new experiments with reactions that were previously not possible. The detector discussed in the following is planned to be used in some of these experiments. The CERN accelerator complex and the ISOLDE facility are shown in figures 1.1 and 1.2.

There are four kinds of reactions of interest for the current detector development. Elastic scattering, inelastic scattering, transfer, and capture reactions, typically on light targets. Elastic scattering can be used to study resonant states, e.g. to investigate cluster states for comparison with nuclear structure models. Transfer reactions are useful to study one nucleon transfer to single particle states and can be used to study how nuclear structure changes towards the drip lines. The results from these experiments can also help to determine reaction rates of interest for nuclear astrophysics [1].

The reactions above can be studied using a thin target by varying the beam energy in small steps, so the incident particles scatter without losing a big portion of their energy. Since it is necessary to increase the beam energy in small steps to get the whole spectrum, the method is very time consuming and costs valuable beam time. By using a thick target the incident beam

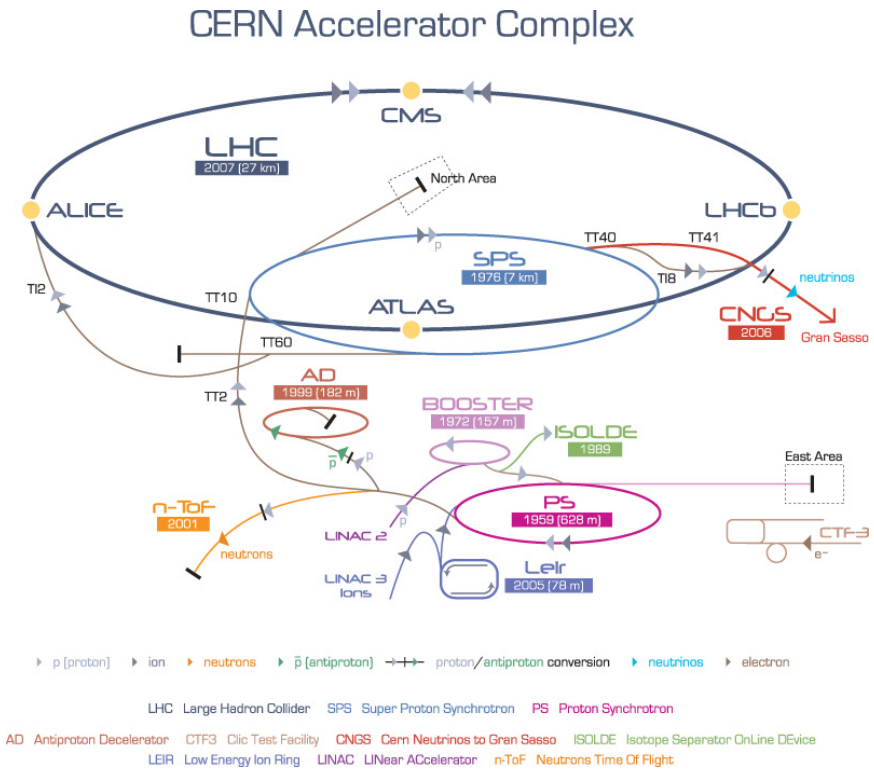

Figure 1.1: CERN accelerator complex. ISOLDE is shown in green. ISOLDE receives protons from the booster.

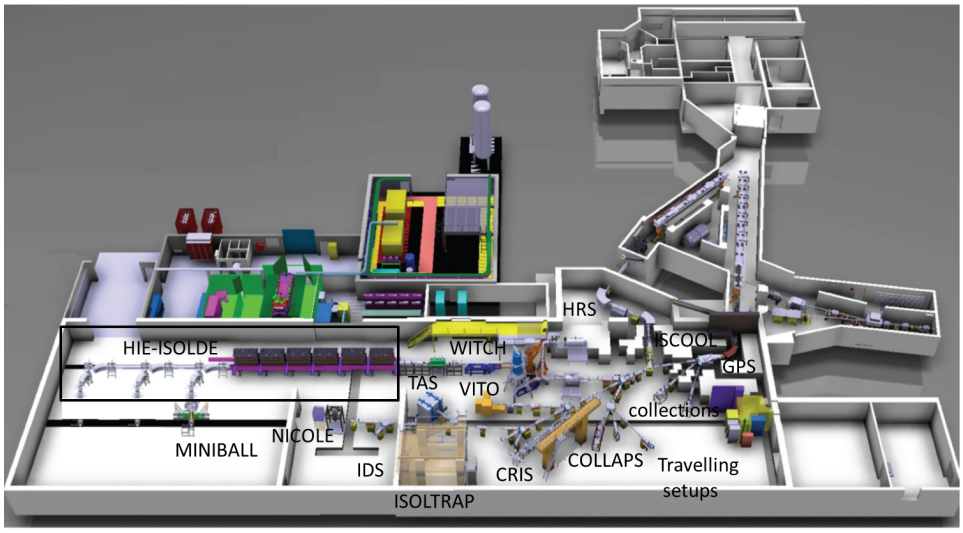

Figure 1.2: Overview of the ISOLDE facility. The new accelerator and beam line for experiments at HIE-ISOLDE is marked with a box to the left.

loses energy by traveling through the medium before and after the reaction. Because of the thickness of the target, reactions that occur at different depth have different interaction energies. These can e.g. be found from simulations and calculations of the stopping power in the target. This method gives poorer resolution compared to a thin target but the beam energy can be increased in much larger steps.

Previous experiments often used a beam of light particles hitting a heavier target, but the experiment can also be performed with a beam of heavy particles hitting a lighter target, usually a gas. The reaction then takes place in inverse kinematics. This technique offers several advantages, the beam can consist of radioactive isotopes that cannot be used as a target. The incoming beam can also be completely stopped in the target making it possible to study all resonant energies in a single run, at the same time as all particles can be detected at forward angles. The disadvantage is that the reactions occur along the beam path and reactions at different distance from the detector will correspond to different scattering angles. The straggling of the beam particles leads to reactions occurring at a specific energy, but at slightly different distances from the detector, decreasing the resolution [2]. This can be solved by using an active target. An active target is e.g. a gaseous ionization detector where the gas atoms also act as the target. The detector can work as a time projection chamber (TPC) and track the incoming beam and the reaction products, which makes it possible to determine the reaction vertex. This in turn makes it possible to measure the angles with high precision which gives the possibility to have a large target without loss in resolution. A schematic of this principle is shown in figure 1.3a. The energy of the beam at the reaction vertex can be measured from the amplitudes of the signals from the TPC and from the length of the track. The specific energy loss in the gas can be used to identify the particles. The gas pressure of the detector can be adjusted to stop the heavy beam particle in the detector while letting the lighter recoils travel through to other detectors at the far end of the volume. This is possible since the beam and reaction products have different specific energy loss in the gas. By stopping the heavy beam ions in the gas, sensitive detectors can be positioned in forward angles close to the beam axis without destroying them. Another advantage is that one can study particle decay in the volume and track the outgoing particles. The choice of operating gas and pressure is determined by the physics case, and the requirement for good working conditions of the detector [1].

1.2 Aim of the thesis

A 3D-model of the detector intended for use as an active target is shown in figure 1.3b. The detector is shown without any readout plane for tracking.

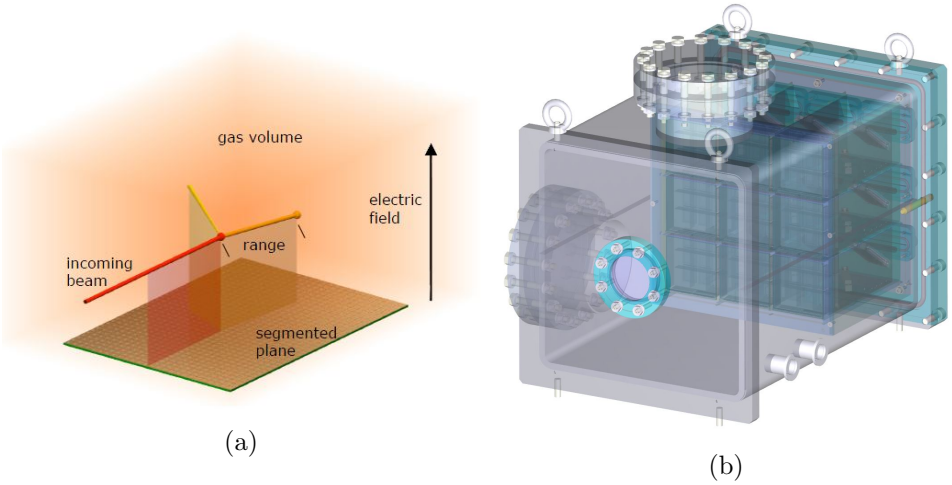

(a) (b)

Figure 1.3: a) Schematics of how a track from an incoming particle is constructed.[1]. b) 3D-model of the scattering chamber. The chamber is shown without the readout plane.

The intention is to use a TPC for tracking of the particles in the detector volume. In addition to a position sensitive readout plane a TPC also needs an electron amplification stage. In the current detector, Gas Electron Multiplier (GEM) foils were chosen as a first solution. The aim of this thesis is therefore to study and characterize GEMs for this purpose. The advantages of using GEM foils compared to other amplification techniques are that they are relatively cheap, easy to manufacture in different shapes, can accept rather high count rates, and are radiation hard. Part of the work is also experience building concerning the handling of GEM foils in a detector setup, the handling has to be done in a clean room environment, which was achieved by assembling, dissembling, and testing a small detector prototype. Several measurements were done to characterize the prototype, including gain measurements, tests with different gas mixtures, and it's long term behavior. The response of the detector has also been simulated using the simulation package Garfield++. The simulations include gain, spread of the electron cloud, and signal response. The simulations and the measurements are compared in order to investigate how well the detector can be modeled using this package.

Chapter 2

Gas detectors

The purpose of a detector in a nuclear physics experiment is to detect incoming radiation and to measure e.g. the energy of the involved particles. This can be achieved through several different techniques. A particle that travels through the detector deposits part of its energy in the detector medium. In most cases the deposited energy is converted to an electrical signal that can be measured. The detector studied in this thesis is a gas detector, i.e. the detection medium is a gas. In this case the radiation is detected by interactions with the gas atoms. The basic principles for these interactions are discussed in the following section.

2.1 Interaction with matter

When a charged particle travels through matter it loses energy. The main fraction of energy loss comes from the electromagnetic interaction between the Coulomb fields of the particle and the atoms in the target material. The particle slows down through multiple inelastic processes of excitation and ionization. The energy loss in each process is often low. The energy loss per unit length in matter is described by the Bethe-Bloch formula 2.1.

$$\frac{dE}{dx} = -\rho \frac{2KZ}{A\beta^2} \left[\ln \left(\frac{2mc^2\beta^2}{I\left(1-\beta^2\right)} \right) - \beta^2 - \frac{C}{Z} - \frac{\delta}{2} \right] \tag{2.1}$$

$$K = \frac{4\pi N e^2}{mc^2} \tag{2.2}$$

where, e and m are the charge and the mass of the electron, Z, A, and ρ the atomic number, mass, and density of the medium, and N is Avogadro's number. The term C/Z comes from inner shell corrections and $\delta/2$ from the density effect correction [3].

Photons on the other hand can interact with matter through three different processes, the photoelectric effect, Compton scattering, and pair production [3].

- **Photoelectric effect:** The photon transfers all energy to an atomic electron. This process is dominant in the low to intermediate energy range. The electron has an energy that is equal to the difference between the incoming photon energy and the binding energy of the electron. There are jumps in the absorption cross section that correspond to the different electronic shells.

- **Compton scattering:** The photon scatter on a quasi-free electron, energy and momentum are conserved.

- **Pair production:** When the photon energy exceeds 1.022 MeV an electron-positron pair can be produced. This process only occurs in the presence of a nucleus to conserve energy and momentum. This is the dominant process for high energy.

The practical domain for photon detection in gas detectors is in the near ultra-violet to the hard X-ray region, because of the low cross section for interactions with photons of higher energies. The dominant process for atomic gases in this region is the photoelectric effect [3].

2.2 Avalanche multiplication

To detect radiation most gaseous detectors use the electrons produced from the interactions with the gas discussed above. To obtain a measurable signal the number of produced electrons needs to be multiplied in order to produce a readable signal. In most gaseous detectors this in done by avalanche multiplication. Avalanche multiplication occurs in gases when the electrons are accelerated by an electric field, E. If the electrons have an energy higher than the ionization potential of the gas atoms or molecules, electron-ion pairs can be produced. The primary and secondary electrons are then accelerated, each producing another electron-ion pair if the energy is sufficient. The number of electrons will then increase exponentially. In a uniform electric field the average multiplication of the number of electrons, M, after a path of length x is given by $M = e^{\alpha x}$, where α is the first Townsend coefficient. It describes the number of produced ion pairs per unit length in different gases and is the inverse of the average distance an electron travels before producing another electron through an ionizing collision. The Townsend coefficient is a function of the reduced field, E/P, where P is the pressure. The electrons have higher velocity in the gas compared to the ions. The charge distribution will therefore have a drop like shape with fast moving electrons in the front and the slower ions at the back [3].

The normalized avalanche size follows a Poisson distribution, where the avalanche probability for N starting electrons is given by equation 2.3, where $x = n/\bar{n}$. n is the exact number of electrons in a given avalanche and, $\bar{n}$,

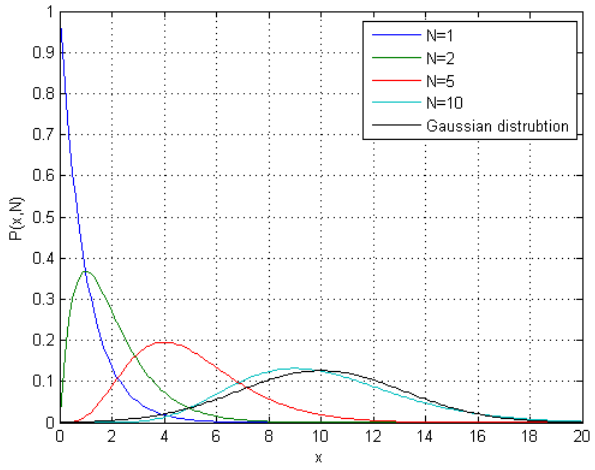

Figure 2.1: Normalized avalanche size probability for different number of starting electrons. The black curve is a Gaussian distribution for N=10

the mean number of electrons in one avalanche.

$$P(x, N) = \frac{x^{N-1}}{(N-1)!} e^{-x} \tag{2.3}$$

Figure 2.1 shows the avalanche probability for different values of the number of starting electrons, N. For large values of N the distribution can be approximated with a Gaussian, as shown for $N = 10$. The spread in the size of the avalanches contributes to the intrinsic energy resolution of gaseous detectors. Further discussion of these distributions are found in [3].

2.2.1 Penning effect

An effect that can increase the multiplication in gases is the Penning effect. This effect is most noticeable if a gas with low ionization potential is added to gas with higher energy excited states. The increase in gain comes from the transformation of excitation energy of an atom of one species to ionization of an atom of another species. If an excited molecule, A^* collides with the molecule B, a free electron can be produced as given by:

$$A^* + B \rightarrow A + B^+ + e^- \tag{2.4}$$

The free electron can then undergo avalanche multiplication and increase the gain of the detector. There can therefore be a benefit of adding a small amount of another gas to the mixture [4].

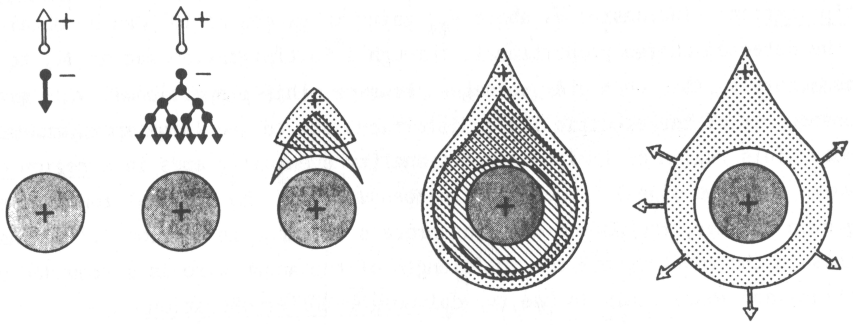

Figure 2.2: Avalanche formation around a wire [3].

2.3 Proportional counter

The first detectors using avalanche multiplication were proportional counters. They exhibit the basic properties of gaseous detectors and are discussed in the following to introduce some general features. A proportional counter consists of a gas filled conducting cylinder with a thin wire on the axis. A high voltage is applied between the cylinder and the wire, with the wire at a positive voltage compared to the cylinder. Electrons produced in the gas will drift towards the anode wire. When the electrons come within a few wire radii of the wire the field is usually large enough to induce avalanche multiplication. The avalanche multiplication around a wire is shown in figure 2.2. The electrons have a larger mobility in the gas compared to the ions and quickly reach the anode wire, while the ions slowly drift towards the cathode cylinder.

By varying the electric field strength the detector behavior changes. The different working regions of a proportional chamber are shown in figure 2.3. With very low field strength the created electron-ion pair will recombine before reaching the wire, while in the ionization region all created charge from the incoming particles are collected. When the field is further increased the electrons begin to undergo avalanche multiplication. The collected charge is then proportional to the number of created electron-ion pairs. At higher field strength the proportionally is lost due to distortions in the fields from the charge induced by the avalanche process. The last region is the Geiger-Müller region. In this region every induced charge gives rise to an equal signal because of continuous avalanches [3].

2.4 Gas medium

The detector characteristics are dependent on the type of gas used. Avalanche multiplications occur in noble gases at much lower electric field than in com-

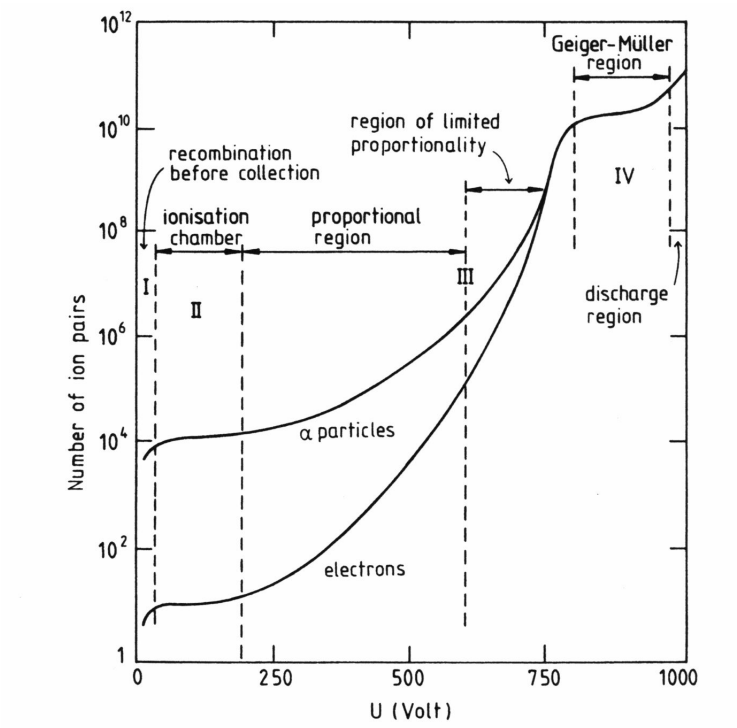

Figure 2.3: The collected charge dependence on the detector voltage. The different working regions are marked [3].

plex molecules, since in the latter case there are more dissipation modes available. If the molecule absorbs energy through vibration or rotation it does not create an electron-ion pair, and avalanche multiplication does not occur. For detection of minimum ionizing particles a high specific ionization, i.e. the number of electron-ion pairs created per unit length of the ionizing particle track, is required. This suggest to use argon, if xenon and krypton are disregarded for being too expensive.

When a noble gas atom has been excited it returns to the ground state by emitting a photon. The emitted photon has an energy that often is above the ionization energy of metals used in e.g. the cathodes. This means that photoelectrons can be extracted. The extracted electrons can then induce another avalanche soon after the first one. This sets a limit for the gain before the detector enters a continuous discharge mode.

The ions created in the avalanche process can release an electron or photon when they recombine. This can also create permanent avalanches. By adding a small amount of a complex molecule that can absorb photons through several different modes, that do not send out an electron, this process can be reduced. Such a molecule acts as a quencher and makes it possible to operate the detector at higher gain. Typical quenchers are carbon dioxide, methane, isobutane etc [3].

2.5 Gas Electron Multiplier

2.5.1 Basic operational principle

The choice of electron amplification technology for the active target detector under development is the Gas Electron Multiplier (GEM). A GEM detector is a micro pattern gaseous detector. The detector consists of one or more thin foils situated in a gas volume. The GEM foils are made of a thin polymer foil coated with copper on both sides. By using photolithographic methods it is possible to make small holes with high density in the foils. Figure 2.4a shows an image of a GEM foil. The foil was photographed with a Nikon Coolpix P6000 through a Nikon eclipse LV100 microscope. A sketch of a GEM foil is shown in figure 2.4b, where the dimensions of a standard foil are indicated. There exists other configurations as well, e.g. thick GEMs where lasers are used to manufacture the holes [3]. The first GEM foils made were used in multiwire proportional chambers, but tests also showed that GEM foils can be used standalone without wire multiplication.

A setup of a GEM detector is shown in figure 2.5. The incoming radiation interacts with the gas and produces electron-ion pairs in the drift region. A suitably selected voltage difference applied between the top foil and the drift cathode makes the electrons drift towards the GEMs. A voltage difference of a few hundred volts between the different sides of the GEM foils gives rise to strong electric fields in the holes. The strong field makes it possible

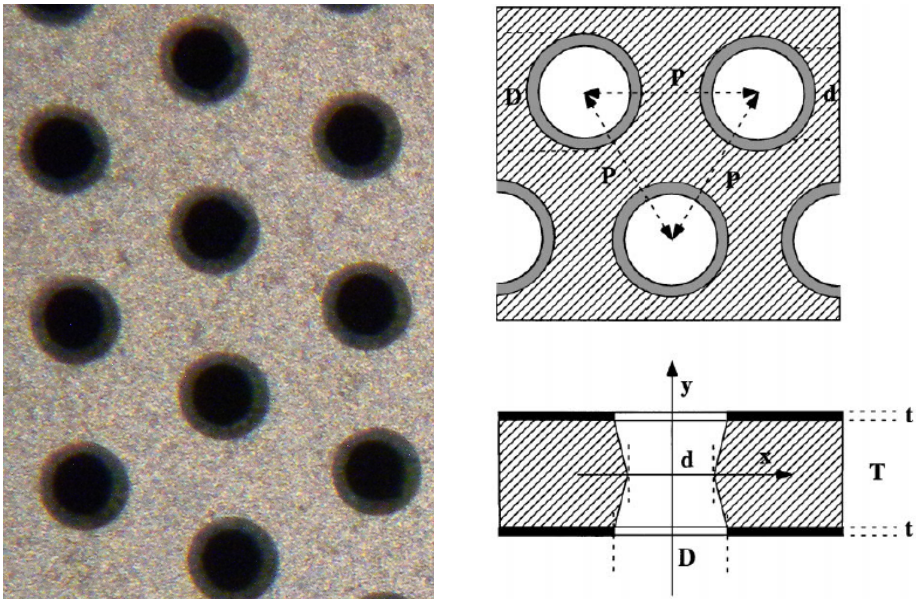

(a) (b)

Figure 2.4: a) A photo of a GEM foil photographed with a Nikon Coolpix P6000 through a Nikon eclipse LV100 microscope. The objective on the microscope had a magnification of 5 times and the image was further zoomed with the optical zoom on the camera. b) Sketch of a GEM foil. The dimensions of a standard foil are, pitch, p = 140 μm, diameters, D = 70 μm, d = 50 μm, thicknesses, T = 50 μm, and, t = 5 μm [5].

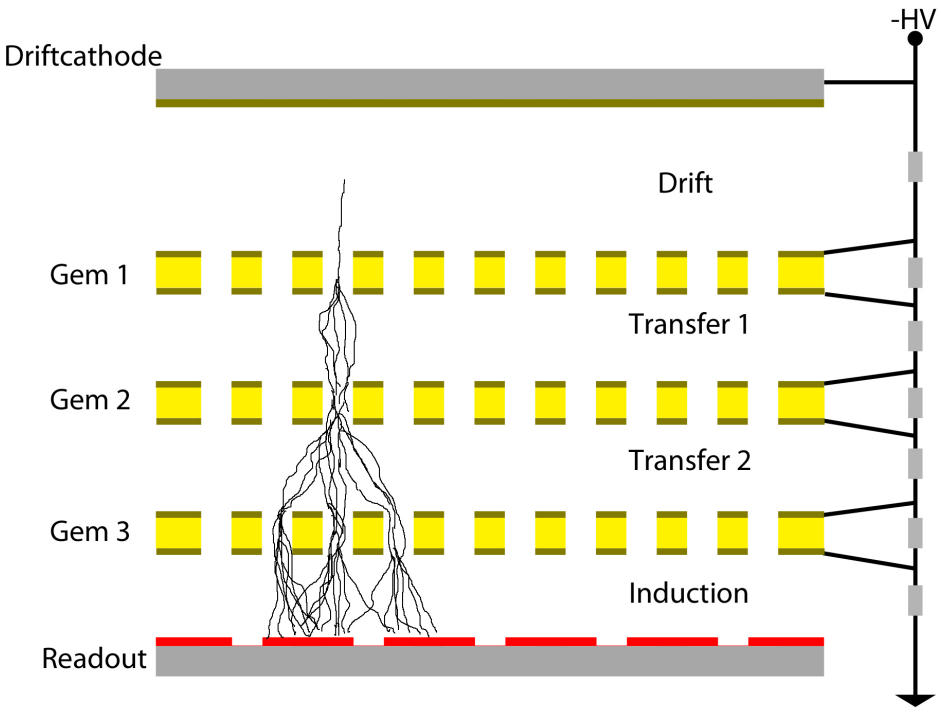

Figure 2.5: Sketch of a GEM detector with the different components. The voltages is applied across each foil with a resistor chain shown to the right, with resistors in grey. The GEM foils are seen in yellow, and the readout plane in red. The black lines sketch how an avalanche could look like.

to achieve avalanche multiplication in the holes, making every hole act as an independent proportional counter. The electric field lines of a GEM electrode can be seen in figure 2.6.

The electrons are extracted from the holes by the electric field between two adjacent foils. After the last foil in the stack, the electrons drift towards the readout plane where they induce a signal. If the voltage across the foil is high enough, it possible to read the signal directly from the PCB board.

Readout

The readout board consists of a segmented electrode. The segmentation makes it possible to determine the position of the incoming particle. The segmentation can be done in different ways, the most common are pads or strips, but the electrodes can also have backgammon shapes where the induced charge is proportional to the position on the pad [1].

The detector is typically powered using a simple resistor chain acting as a voltage divider [7]. By stacking several foils on top of each other it possible to further increase the gain of the detector. The distance between

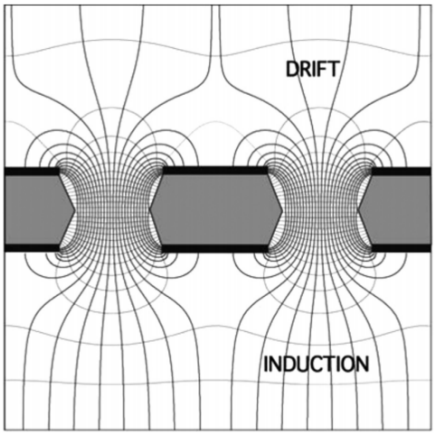

Figure 2.6: Electric field lines on a gem electrode. The thin horizontal lines are equipotentials [6].

two foils is typically around 0.5-3 mm. The transfer field across each gap is also provided by the voltage divider. Typical fields are 2-3 kV/cm. The gain of the whole detector is then equal to the product of the gain of each single foil.

2.5.2 Configurations

If several foils are stacked the detector can be operated at a high total gain at a lower voltage across each foil, which leads to a lower risk of discharge. The configuration of voltages applied over the foils has an impact on the characteristics of the detector. The configuration that is experimentally shown to minimize the risk of discharge is called the standard configuration in the following [8]. In this case the resistors are chosen so that the highest applied voltage is across the top GEM foil, while decreasing over the other foils. In a triple GEM stack the voltage on the top foil is $\sim 10\%$ higher compared to the middle foil, and similarly the voltage on the bottom foil is $\sim 10\%$ lower compared to the middle foil [8]. In contrast, the configuration that minimizes the number of ions that drift through the detector into the drift volume is the opposite, with the lowest voltage across the top foil [9].

2.5.3 Gain

The effective gain of a GEM detector is defined as the number of electrons that reach the readout plane for each primary electron produced. This number can be obtained by measuring the current on the readout board. As the current is the product of the number of primaries created by the incoming particle, the interaction rate, the electron charge, and the gain of the detector, it can be expressed as:

$$I = e \cdot n_p \cdot f^* \cdot G \tag{2.5}$$

where, I is the induced current on the readout plane, e the electron charge, n_p the number of primaries generated by an incoming particle, f^* the measured interaction rate, and G the gain [9]. The interaction rate f^* is obtain by plotting the count rate against the voltage across the foils. For low voltages not all electrons created are collected. When the voltage increases the fraction of events that are registered increases. For high enough voltage all events are detected and the rate reaches a plateau, which corresponds to the interaction rate. The number of primaries generated, n_p, depends on the incoming type of radiation, the energy, and the gas medium. Due to known cross sections for the processes described in section 2.1, the number of primaries can be determined through simulations. By measuring the current it is therefore possible to deduce G. The gain can then be used to compare different configurations. Additional features that can be of interest to compare between different configurations are, the spread of the electron cloud when it reaches the readout board and the time structure of the signal.

2.5.4 Geometrical effects

The gain also depends on the geometry of the holes. The gain decreases with increasing hole diameter but reaches a plateau at a diameter of 70 µm and does not increase with a smaller diameter [10]. The pitch has no influence on the gain but affects the collection efficiency.

Depositing of charge on the insulator inside of the holes and polarization of the polymer lead to changes in the electric field inside the holes, which results in changes in the gain of the detector over time [11]. The shape of the holes also affects the charging up of the foils. This charge up effect increases with a more conical hole, i.e. decreasing inner diameter compared to the outer diameter. This is due to increasing surface area of the insulator. The time it takes for the foils to charge up is dependent on the hole shape and rate of the incoming radiation. If on the other hand the holes are cylindrical in shape with equal inner and outer diameter there is no charging up [10].

2.5.5 Other characteristics

Since the charge multiplication only takes place in the holes, it is independent of the shape of the foils, which makes it possible to shape the foils to match experimental requirements. It is e.g. possible to make non-planar detectors [3].

The high density of holes in a GEM means that the spatial resolution is only limited by the electron spread due to diffusion [7]. A further advantage with GEM detectors is that they give fast signals with a very small ion diffusion tail. This is due to the ions being created in the holes and then

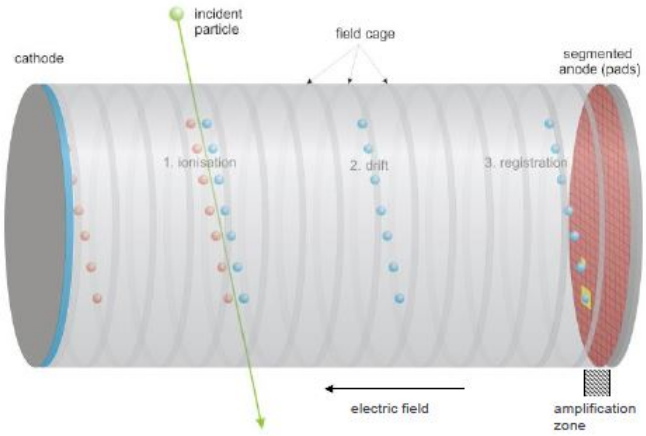

Figure 2.7: Schematics of a TPC. The different steps for track construction is shown [1].

traveling to the opposite side of the GEM foil. The positive ions are thus collected on the top side of the foils screening the ions from influencing the detected signal at the readout plane [12].

2.6 Time projection chamber

The final goal is to produce a TPC for tracking of particles involved in nuclear physics reactions. The schematics of a cylindrical TPC can be seen in figure 2.7. The incoming particles ionize, as discussed above, the gas atoms in the chamber and produce electron-ion pairs, that drift towards the anode and cathode due to an applied electric field. Finally the amplified electrons induce a signal on the readout plane. This creates a two dimensional projection of the track. The drift time of the electrons is measured and used to construct the third dimension. The timing can be deduced in three different ways, internal triggering, using the time structure of the beam, or by external detectors. Internal triggering uses the relative time from the first detected event in the readout plane, which is assumed to have occurred along the beam axis. The other methods use the internal time structure of the beam or a signal from an external detector, respectively.

Chapter 3

Method and measurements

This chapter discusses the assembly and measurements performed on a small prototype detector in order to test the GEM foils. The measurements were done in the following steps:

- Testing of individual foils and assembling of the detector,
- measuring the rate curve and current to find the gain and resolution of the detector,
- testing the detector with several different mixtures of argon and carbon dioxide,
- test how the detector responds to a gradual leak,
- investigating the long term behavior and charging up of the foils.

3.1 Assembly

The GEM foils are sensitive to dust. If there is dust in the holes it can short circuit the two sides of the foils and produce discharges, which can damage the foils. To prevent this all handling of exposed foils has to be done in a clean room. For the work here a clean room at Lund Nano Lab and a clean room at CERN was used.

The foils have the standard dimensions given in figure 2.4b and an active area of 10×10 cm^2. They are mounted in an epoxy frame with a thickness of 0.5 mm on each side of the foil, as can be seen in figure 3.1a. Each foil has two fan outs that is used to connect the foil to the readout board. The readout plane used in the detector consisted of 256×256 strips. In figure 3.1b a readout board of the pad type is shown. The foils are mounted on four nylon screws marked with white circles in the figure and are connected to the readout board by soldering the fan outs to the connections shown in the top and left of the figure. To adjust the distances between each foil 0.5

mm thick spacers were used. The detector was assembled with three foils. The distance between each foil and the readout board was 2 mm and the drift region was 3 mm thick. Figure 3.1e shows a side view of the mounted foils. The gas volume of the detector is formed by the frame shown in figure 3.1c. Gas inlet and outlet is connected to the detector through two quick connectors mounted in the frame. The frame was mounted on the readout board as shown in figure 3.1f covering a square with sides ca 1 cm larger compared to the GEM foils. The volume was closed with a plate (see figure 3.1d). To form a gas tight seal, o-rings were placed between the frame and readout board, and top plate, respectively. The lid has a 50 μm kapton window to let incoming radiation through.

Before and after soldering the foils to the board they were tested to make sure that they worked properly. First the capacitance of each foil was measured. For a 10×10 cm^2 foil the capacitance should be around 5.8 nF. A voltage of $\sim$ 600 V was then applied to the foils to test for discharges (a foil test is shown in figure 3.2). The test time was ca 1 minute. During this period the current was measured to ensure it did not exceed 10 nA. It is possible to have discharges during conditioning but the rate should rapidly decrease and finally completely vanish. In summary the conditioning of the foils was performed in the following steps:

- Visual inspection of the foil,
- capacitance and current test of the foil,
- mounting the foil on the board and protecting it while soldering the connections,
- capacitance and current test of the foil through the connections on the readout board.

This procedure was repeated for all foils in a stack and redone when foils were replaced. After a foil is soldered to the board all mounted foils are tested to make sure that they are still functioning. A gas leakage test was also performed on the assembled detector. To prevent leaks the nylon screw heads was sealed with glue.

3.2 Setup

Two different setups were used, one in Lund and one at CERN. The long time measurement was done in Lund and the other measurements were carried out at CERN. In Lund the detector was put inside a metal box acting as a Farady cage. The different setups can be seen in figure 3.3.

The potentials on the foils needs to be set to make the electrons drift through the detector. The high voltage was connected to a voltage divider

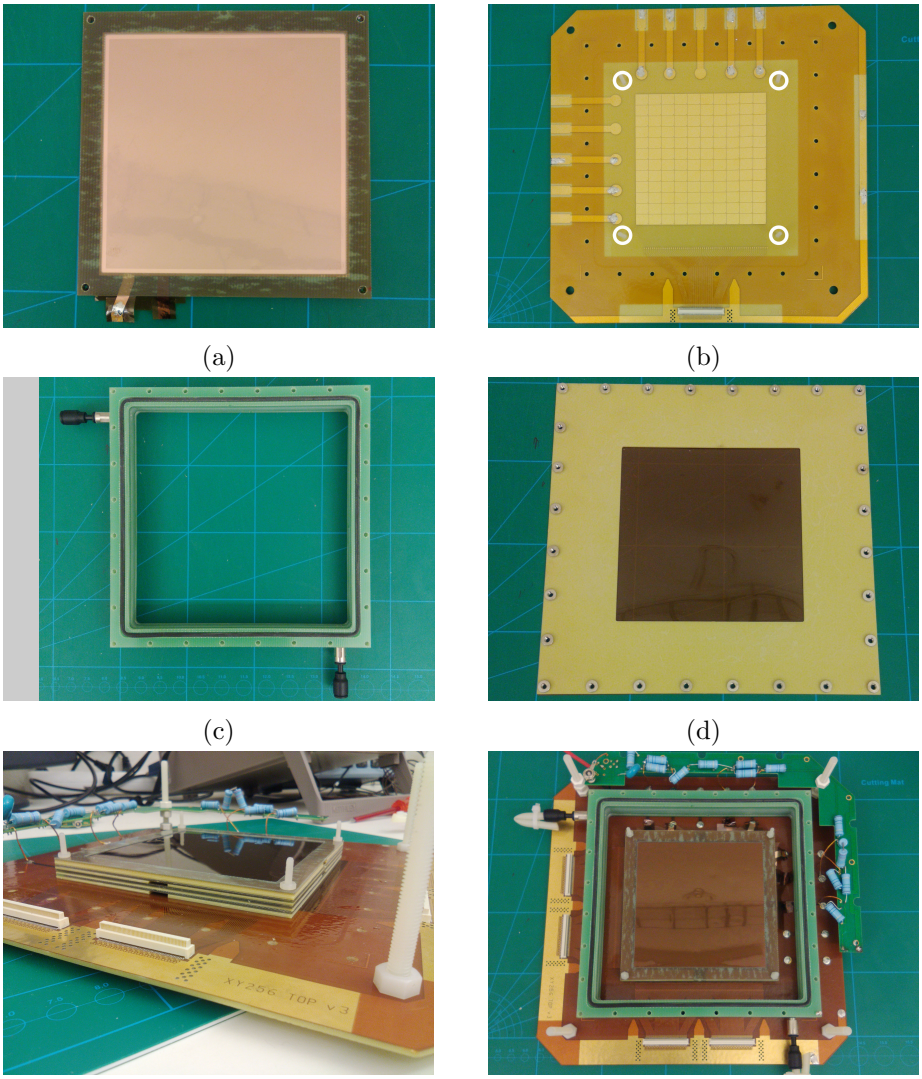

Figure 3.1: a) A single GEM foil with an active area of $10 \times 10\text{cm}^2$. Part of the fan-outs used to connect the foil to the readout board is shown in the lower left corner. b) A readout board of the pad type. The plane consists of 10×10 pads. The strips to connect the GEM foils is shown to the top and left. The white circles marks the nylon screws used to mount the foils. The board is $\sim 25 \times 25$ cm^2 c) Frame for construction of the detector volume. The gas connections is shown. d) Lid for the detector. A kapton window is used to let radiation enter the detector. e) Side view of the foils mounted to the readout board. The spacers can be seen in yellow. f) Top view of the detector with the frame mounted.

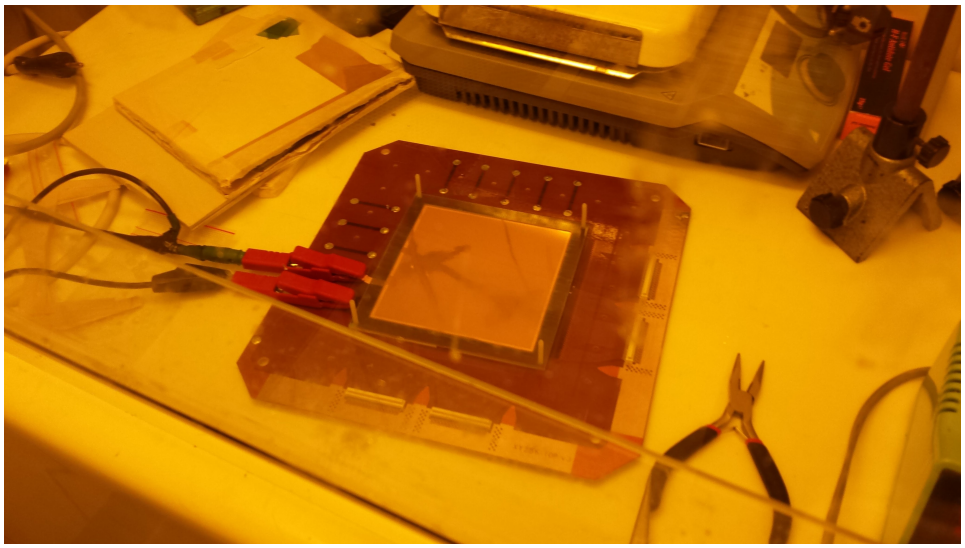

Figure 3.2: Current test of the foils. A voltage of 600 V is connected to the fan outs of the foils.

consisting of a resistor chain. The values of the resistors across the GEM foils were 550, 500, and 450 kΩ. The voltage over each GEM is decreasing and the difference from the middle foil is ∼10%, which minimizes the discharge probability as discussed in section 2.5.2. The resistors across the drift, transfer, and induction region had a value of 1 MΩ. A sketch of the voltage divider is shown in figure 3.4. During the measurements at CERN a filter was also connected in series before the voltage divider. This was done to reduce the noise coming from the high voltage supply. The voltage divider was connected to the top of each GEM foil and to the drift foil via 10 MΩ resistors and connected directly to the bottom of each foil. The 10 MΩ resistors are used to protect the detector in case of a short circuit in one of the foils. If a short circuit occurs in a foil the resistor across the foil will be connected in parallel with the high value resistor. This means that the voltage drop across the resistor will almost be the same as before the short circuit. The whole foil will then have the same potential as the bottom of the foil before the short circuit. Because of the resistor the voltage increase over the other GEM foils will be minimized, preventing further discharges. This also minimizes the increase in the electric fields in the gaps between foils. The signal for the measurements was taken from the bottom of the third GEM foil, via a capacitor to disconnect the preamplifier from the high voltage. The current measurement was done on the readout plane. The induced signal on the bottom of the last foil is equal, but with the opposite sign to the signal from the readout plane. All the strips on the readout plane were summed for the current measurement. To reduce the noise the detector

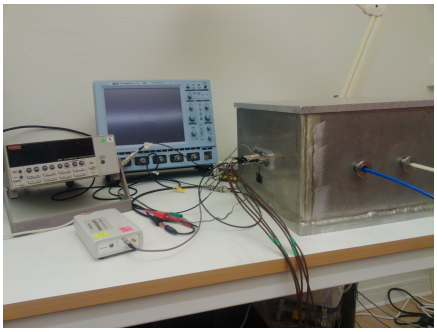

(a)

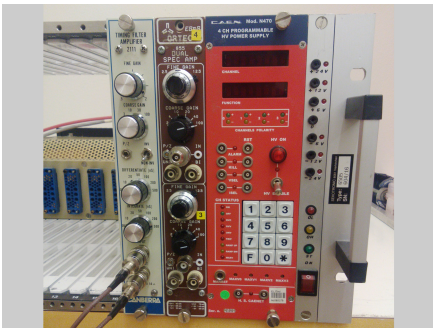

(b)

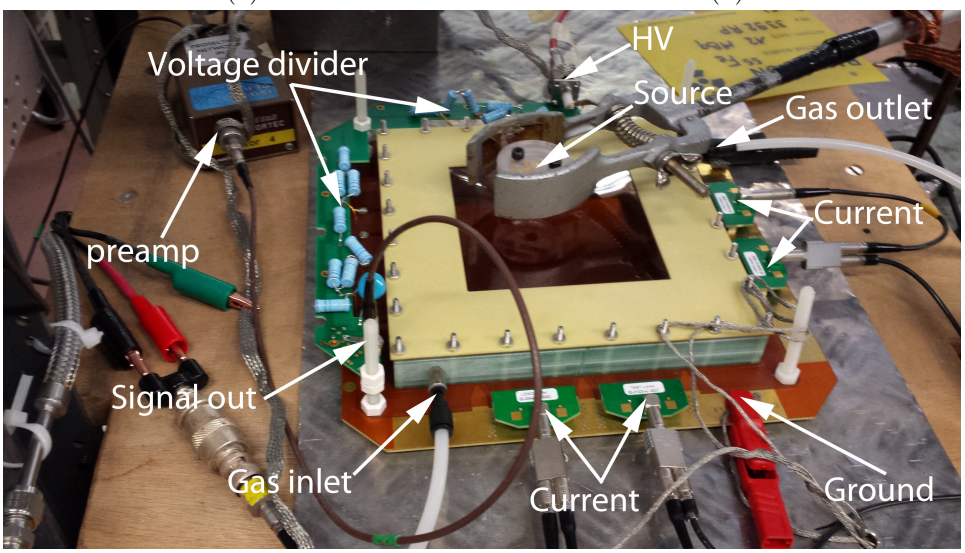

(c)

Figure 3.3: a) Setup used in Lund. A Keithley 6487 picoammeter with the MCA in front is shown to the left. The detector is placed inside the metal box for noise reduction. b) A high voltage supply of model CAEN N470 was used to power the detector. The preamp was connected to a Canberra 2111 TFA. c) Setup used at CERN. The different components are labeled in the figure.

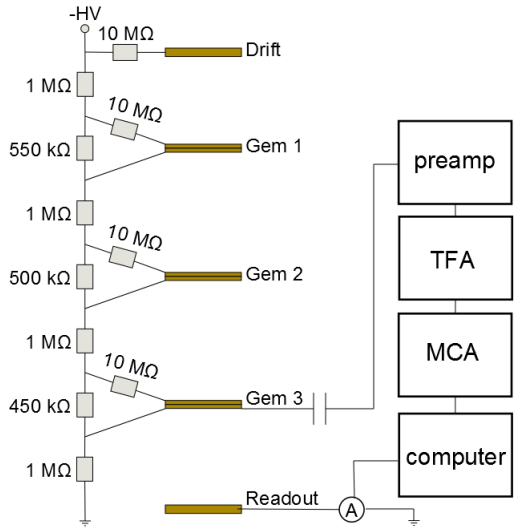

Figure 3.4: The voltage divider used in the measurements. The electronics connections is shown in the boxes.

was properly grounded, which required a substantial effort, and during the long time measurement placed inside a metal box acting as a Faraday cage. During the measurements the signal to noise ratio was about ten to one.

3.3 Measurement details

All the measurements were done with a ^{55}Fe source. The signal was brought via an Ortec 142 preamplifer to a Canberra 2111 timing filter amplifier and finally to an MCA connected to a PC where the spectrum was recorded. The settings on the TFA was 20 ns differentiation, 500 ns integration, coarse gain at 100, and fine gain at 2. The current was measured with a Keithley 6487 picoammeter and recorded with a Labview program via a GPIB interface. The high voltage supply used was CAEN N470. The voltage given on the x-axis in figures 3.5 and 3.6 is the total voltage across the detector and the filter. The corresponding voltages across each GEM foil, the drift gap, transfer gaps, and the induction gap are given in table 3.1.

3.3.1 Gases

The detector has been tested with three different mixtures of Ar and CO_2 in the ratios, 70/30, 76/24, and 82/18 with a gas flow of 4-5 l/h. The rate plots for the different gases are shown in figure 3.5 (for further discussion see chapter 5). The number of events over a set threshold (at channel 225) was

Table 3.1: Voltages across the different regions

Total voltage	ΔV_{Gap}	ΔV_{Gem1}	ΔV_{Gem2}	ΔV_{Gem3}
3600	621	341	310	279
3700	638	351	319	287
3800	655	360	328	295
3900	672	370	336	303
4000	690	379	345	310
4100	707	389	353	318

counted using the MCA. For each voltage two spectra were taken, one with the source and one without for the background. Each measurement was done during 30 seconds. For the background measurement the source was blocked by inserting a metal sheet between the detector and the source. The measured rate, by this method, was compared to that using an oscilloscope to ensure consistency. As part the analysis the rate curve was fitted with the following model:

$$y = \frac{a}{1 + exp(-b(x - c))} \tag{3.1}$$

where a, b, and c are fit parameters that describe the values at the plateau, the slope, and the midpoint of the slope, respectively. The curve was fitted to the data using the MATLAB fit function. The rate plateaus, giving f^* in equation 2.5 for the different gases are with 95 percent confidence limits 832.3±12.3 Hz, 1111±29 Hz, and 963.2±37.8 Hz, with a turnover point at ca 4000 V, 3850 V, and 3700 V.

The current from the detector was continuously recorded during the rate measurements. The measured current for an Ar/CO_2 ratio of 76/24 is shown in figure 3.5d. The wider bands correspond to measurements with source, and the narrower ones to background measurements. The large spikes in the figure correspond to changing the high voltage across the detector. Each high voltage value is paired with the measured current using the time sequence together with logbook entries. The current is averaged and the background is subtracted before the gain is calculated. The rate, the current, and the number of primaries were then used to calculate the gain, according to equation 2.5, which is plotted for different gas mixtures in figure 3.6. The simulations of the number of primaries are described in section 4.4. The gain for the different gas mixtures is shown in figure 3.6, and varies between ca 1500 and 15000 at 4000 V. One should note that the maximum safe operational voltage that can be applied is limited by the risk of foil breakdown or discharges inside the detector.

The spectrum for ^{55}Fe for the different gas mixtures is shown in figure 3.6. This spectrum was taken at voltages of 4100 V, 3950 V, and 3780 V to have similar gain. The resolution of each spectrum is measured by fitting a

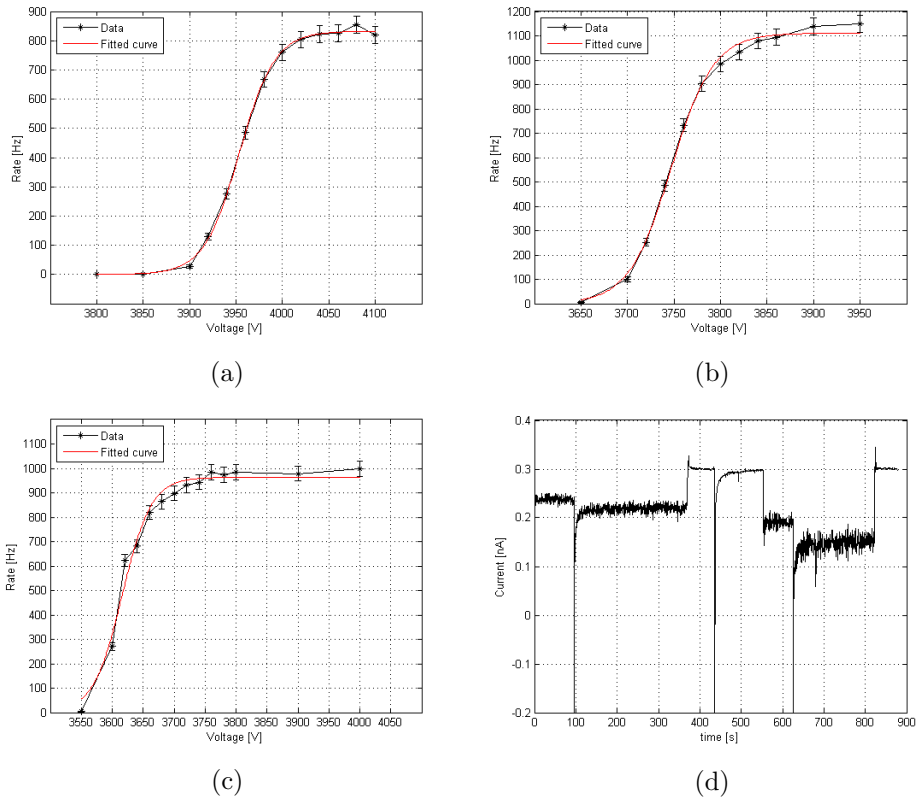

Figure 3.5: a)-c) shows the rate curves for the different gas mixtures of Ar/CO_2, 70/30, 76/24, and 82/18. d) shows the current measurement for the gas mixture Ar/CO_2 76/24. All measurements was done with an ^{55}Fe source.

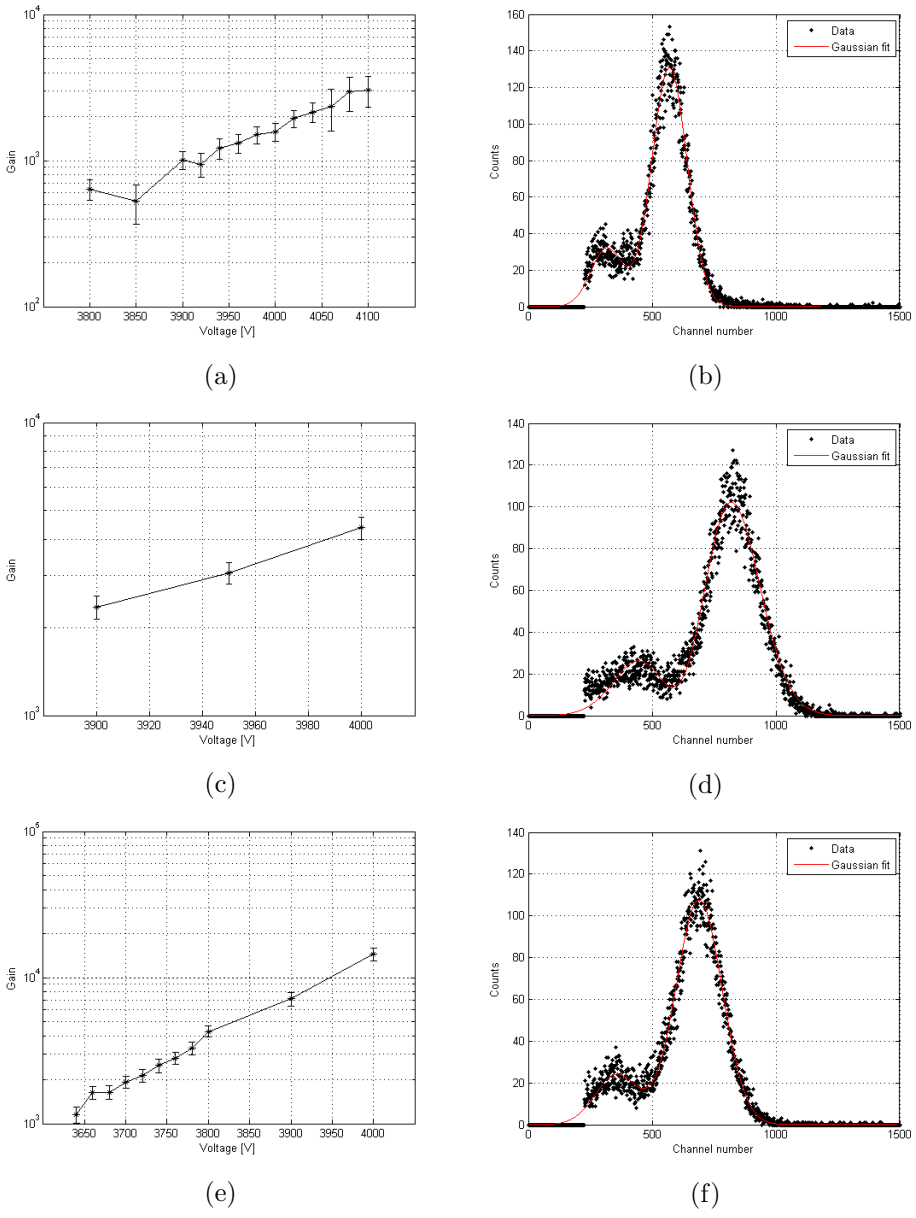

Figure 3.6: The left panels show the gain for of a triple GEM in the standard configuration for the same gas mixtures as in figure 3.5. The right panels show the spectra for the same gas mixtures, taken at 4100 V, 3950 V, and 3780 V. See discussion in text.

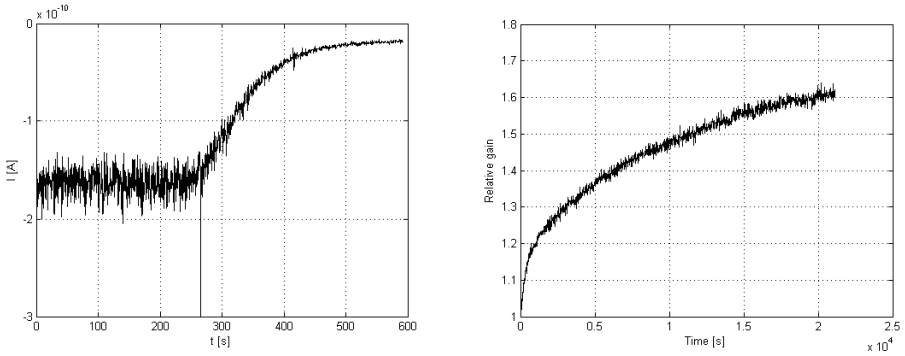

(a) (b)

Figure 3.7: a) Current measured during the gas leakage test as a function of time. The voltage across the detector was 4200 V. b) The change of gain over time, showing the charging up of the detector. The measurement was done at 4000 V.

sum of two Gaussian functions to the data, one for the argon escape peak and one for the full energy peak. The resolution was 16 %, 33 %, and 23 % for the three cases, which is in line with expectation.

3.3.2 Leakage test

The initial gas mixture for this test was argon and carbon dioxide in the ratio 70 to 30. The measurements were done with a voltage of 4200 V. To study the effects of a gas leak in the detector, the argon was turned off while the carbon dioxide was left on. The flow through the detector decreased to half of the initial flow when the argon was turned off. The measured current, that is directly proportional to the gain, is shown in figure 3.7a. At this leakage rate it took about three minutes before the gain went to zero. One can also note that the change is not linear with time.

3.3.3 Long duration measurement

It is also relevant to study how the performance of the detector changes during long measurements. Specifically, if there are charge up effects, how long time it takes before the detector has stabilized. This test was done with an applied voltage of 3800 V without filter in front of the voltage divider. The voltage across each foil is given in the 4000 V row in table 3.1. The gas mixture was Ar/CO_2 in the ratio 82/18. A ^{55}Fe source rate of ~ 5 kHz was used. The results of the measurements are shown in figure 3.7b. The relative gain is calculated by dividing each measurement with the mean of the first 20 measured currents. Under these conditions it took ca 5 hours before the gain stabilized at approximately 1.6 times the initial value.

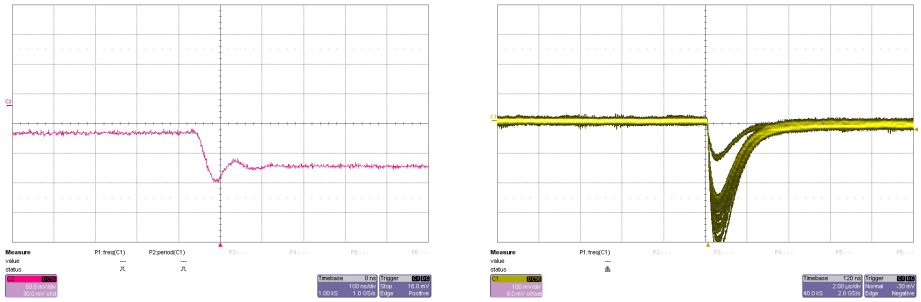

(a) (b)

Figure 3.8: Measured signals from the detector. The signals were recorded with a LeCroy WaveSurfer 454 oscilloscope. a) Signal after a Ortec 142 preamplifier. b) Signal after a Canberra 2111 TFA and the preamplifier. The argon escape peak can be seen with roughly half of the full signal amplitude.

3.3.4 Signal measurement

The purpose of this measurement was to see how well the signal amplitude from the detector matches the input range of future data acquisition systems, where the maximum input amplitude is expected to be 1 V. A second purpose was to make an attempt to study the collection of the generated charge, from one event on the readout plane, with a final aim to investigate if one can compare the measured signals to simulated ones.

Signals after the preamplifier and the TFA stages, respectively, are shown in figure 3.8. The same voltages across the detector were used here as in the previous section. The signals were recorded by a LeCroy WaveSurfer 454 oscilloscope. To detect the signal after the preamplifier the oscilloscope triggered on the timing output of the preamplifier connected to the TFA. The argon escape peak (see section 4.4) can be seen at roughly half of the amplitude of the 5.9 keV full energy peak, in figure 3.8b. The signal amplitude from the preamplifier was in the 100 mV range, and with the settings previously mentioned the signal amplitude after the TFA was ca 500 mV. The rise time of the signal after the preamplifier was ca 30 ns. Due to noise it was difficult to reliably measure the fall time (in the µs range) of the preamplifier signal.

3.3.5 Signal response and Bode diagram

To calculate the output signal from a simulated input signal the system response, i.e. the response of the amplification stages needs to be known. The system can be represented by a black box, where the input signal is transferred, using a transfer function $\mathcal{H}$, to the output signal (see figure 3.9). Assuming $\mathcal{H}$ is known this model enables the calculation of the output

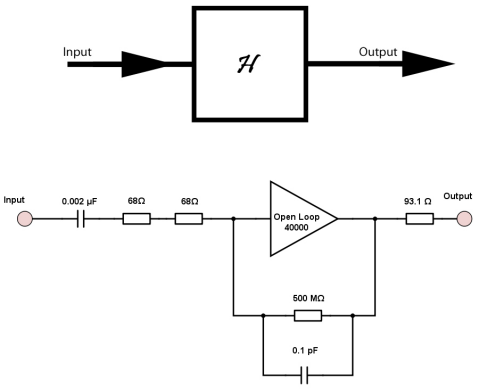

Figure 3.9: Black box model of the system. The circuit diagram of An Ortec 142 preamplifier is shown in the bottom part.

signals without exact knowledge of the circuits in the amplifiers. $\mathcal{H}$ can be determined by measuring the amplitude and phase response as a function of frequency using a spectrum analyzer. This information can be presented in a Bode diagram, which consists of two different plots. The first shows the amplification of the input signal through the system. The vertical axis of this plot is usually presented in dB scale, where dB is calculated as $\text{dB} = 20 \cdot \log_{10}(\text{Gain})$. The second shows the phase difference as a function of frequency between the input and output signal of the system.

Experimentally the Bode diagram is determined by sending sine signals of different frequencies through the system while measuring the change in amplitude and phase between the input and output signal. As a first test the response was measured both for a single Ortec 142 preamplifier and for the preamplifier connected to the Canberra 2111 TFA, with the settings described above. The analyzer was calibrated for coaxial cables using the Q5001 standard, in order to only measure the response for the amplifiers and not the cables. The Bode diagrams for the two different setups are shown in figure 3.10. The magnitude plot for the preamplifier shows that amplification only occurs for frequencies below $\sim$100 MHz. The combined system has a more complicated magnitude plot, where the amplification drops to one at ca 25 MHz and then again slightly rises before falling to one at ca $\sim$100 MHz.

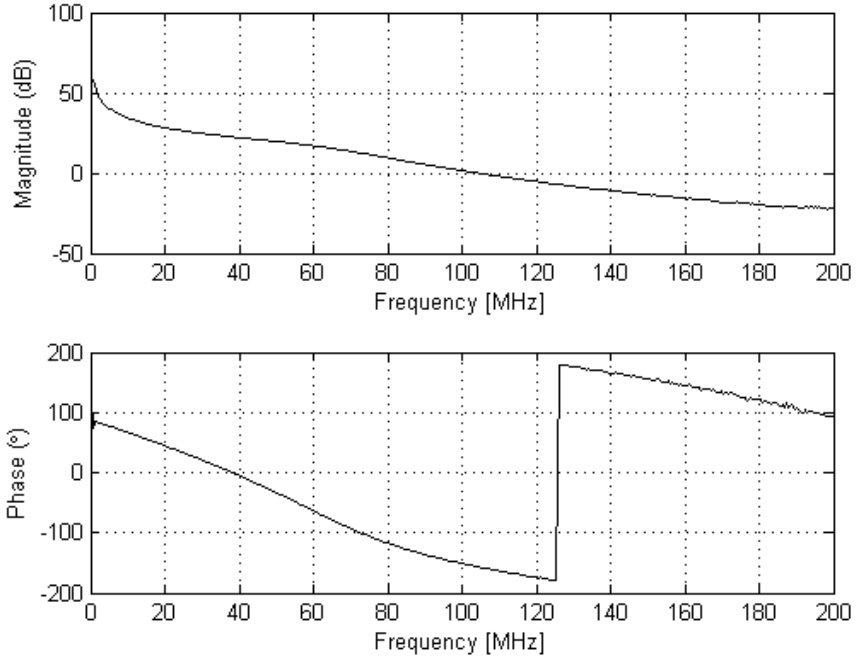

(a)

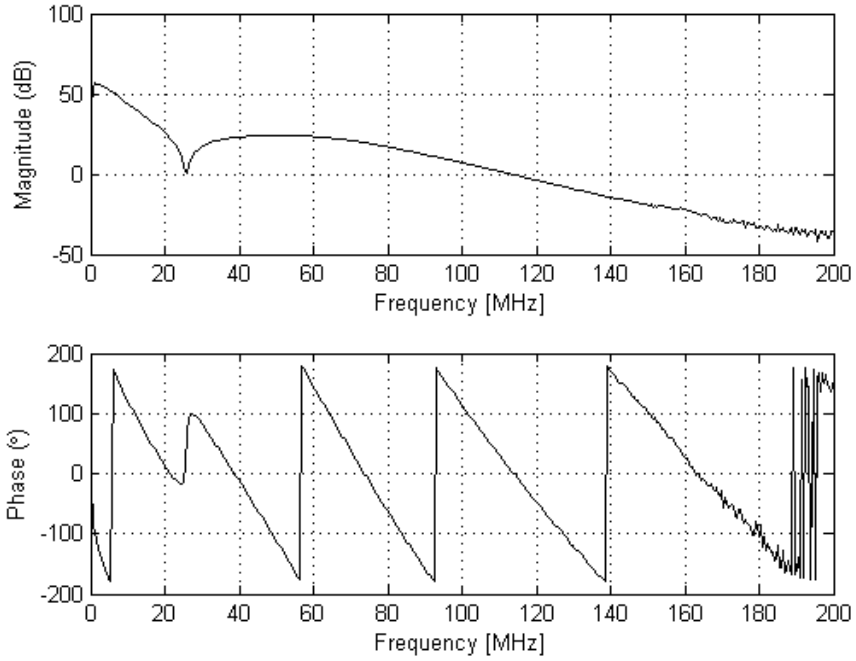

(b)

Figure 3.10: Bode diagrams for the electronics. a) Bode plot for the Ortec 142 preamplifier. b) Bode plot for the preamplifier connected to the TFA. The diagrams were measured from 10 kHz to 200.01 MHz.

Chapter 4

Simulations

Simulations were performed in order to compare the results of the previous chapter with a model built in the simulation package Garfield++. The idea is to benchmark the simulations before future application of the package for use in the final detector design. Garfield++ was also used to simulate the number primaries generated by the incoming radiation. Due to the computing power required for the simulations they were performed on the Iridium cluster at Lund University with a running time of up to five days.

The simulations required a combination of several different programs namely:

- Gmsh to create the geometry of the detector and the meshing needed for the field calculations,
- Elmer to solve the electric fields in the detector and for graphical visualization of the potentials,
- Garfield++ to simulate particle interactions with the gas and avalanche creation.

The following sections will describe each program in more detail.

4.1 Garfield++

Garfield++ is a simulation package specifically made for simulation of gaseous detectors. Simple electric fields can be constructed with the package, but more complex fields must be solved by an external solver. In the current case the electric fields used in the simulations were solved by the open source finite element program Elmer [13]. The fields were then read into Garfield++ using an interface. Garfield++ uses two other packages, Heed and Magboltz to calculate the properties of gas mixtures and the electron transport properties for a given electric field. The avalanches were studied with a microscopic

transport and avalanche method. It uses the drift velocity, diffusion properties, and the Townsend coefficient calculated by Magboltz to describe the avalanches on a molecular level. The method keeps track of the created electrons and their positions. The Penning effect (see section 2.2.1) is also taken in account for the calculations of the gas gain [14]. In summary, Garfield++ was used to simulate the number of primaries generated in the drift volume, the gain of the detector, the induced signal and the spread of the electron cloud at the readout plane. All the simulations were carried out with gases at a temperature of 20 °C and a pressure of 1 atm.

4.2 Elmer and Gmsh

As mentioned above Garfield++ requires that the electric field is solved using an external finite element solver that in turn requires a mesh. The mesh was created using the program Gmsh[15]. In the following a brief discussion of the finite element method is given for completeness.

4.2.1 Finite Element Method

The Finite Element Method (FEM) is a numerical method to solve differential equations. For the simulation of the GEM the electric potential, ϕ, is calculated using Laplace's equation:

$$\nabla^2\phi = 0 \tag{4.1}$$

In FEM [16] the body, in which the equation is solved is divided into several small elements, where each element contains a number of nodes. The function, ϕ, is approximated by basis functions between the nodes in each element. To obtain the FEM formulation the differential equation is rewritten into its weak form, the basis functions are chosen, and the weighting functions are approximated. The basis functions are often polynomials. The problems then takes the form of a system of linear equations, with the number of equations equal to the number of nodes. The system is solved for the nodal values, by insertion of the boundary conditions. The nodal values can then be used to obtain an approximation for the whole problem region.

The elements used can be of various types, the simplest three dimensional element is a tetrahedron shape with a node in each corner. Garfield++ uses second order elements that also have a node on the midpoint of each side of the tetrahedron.

4.3 Electric fields

The geometry of the GEM detector was modeled in Gmsh. Due to symmetry it is sufficient to solve the field for two quarters of a hole only, to minimize

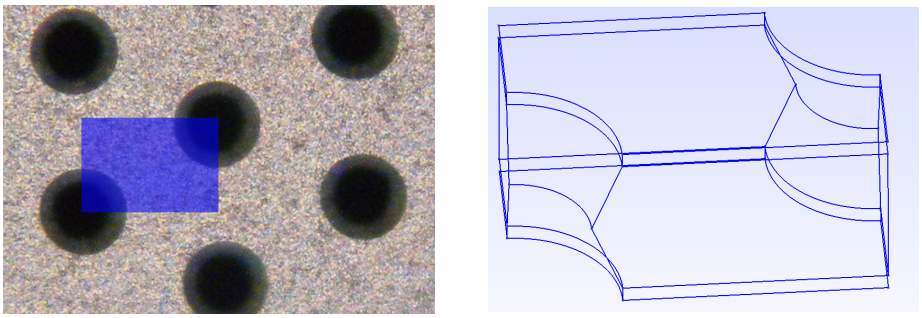

(a) (b)

Figure 4.1: a) The modeled area of the GEM is shown in blue. The fields are mirrored to cover the whole area. b) A GEM foil constructed in Gmsh.

the number of calculations. The field is mirrored in the plane to form the detector foil. The selected volume is shown in figure 4.1a and an image of the geometry of the GEM created using Gmsh is shown in figure 4.1b. The GEM foils used in the simulation have a hole pitch of 140 µm, an outer hole diameter of 70 µm, and an inner hole diameter of 50 µm. Isosurfaces of the potential across a single GEM foil was calculated and is presented in figure 4.2. The figure, plotted using Elmer, is for a voltage across the foil of 400 V. The equipotental surfaces have the expected appearance when comparing to the literature (figure 2.6). The isosurfaces are almost planar in the center of the holes, but bend significantly close to surfaces of the foil.

4.4 Number of primaries

To be able to calculate the effective gain from the detector according to equation 2.5 the number of primaries generated by an incoming particle needs to be known. The source used in the measurements was ^{55}Fe, which decays by electron capture followed by the emission of a 5.9 keV gamma ray. To simulate the number of primaries created from the source, photons with the energy of 5.9 keV were injected into a gas volume, modeled in Garfield++, with the size $0.3 \times 20 \times 20$ cm^3.

The filling gas was a mixture of argon and carbon dioxide in the ratio 70/30. When photons interacts with the gas through the processes described in section 2.1 delta electrons are produced. Garfield++ has built-in functions that keep track of, and counts, the number of produced electrons. A simulation with 10 million photons resulted in the distribution shown in figure 4.3.

The spectrum shows two distinct peaks. One at 209.5 ± 6.31 generated electrons and one at 96.78 ± 4.58 generated electrons. The smaller peak corresponds to the argon escape peak. In this case a K electron in argon,

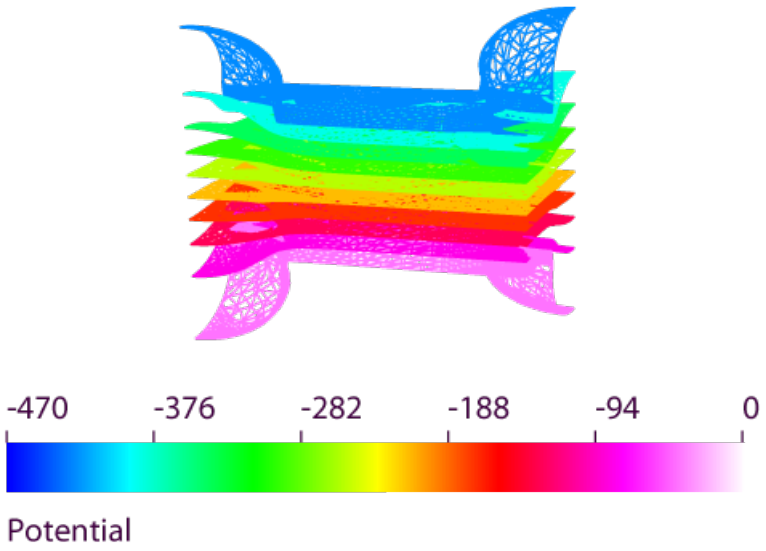

Figure 4.2: Isosurfaces of the potential across a single GEM. The potential across the GEM is 400 V. For geometry compare to figure 4.1

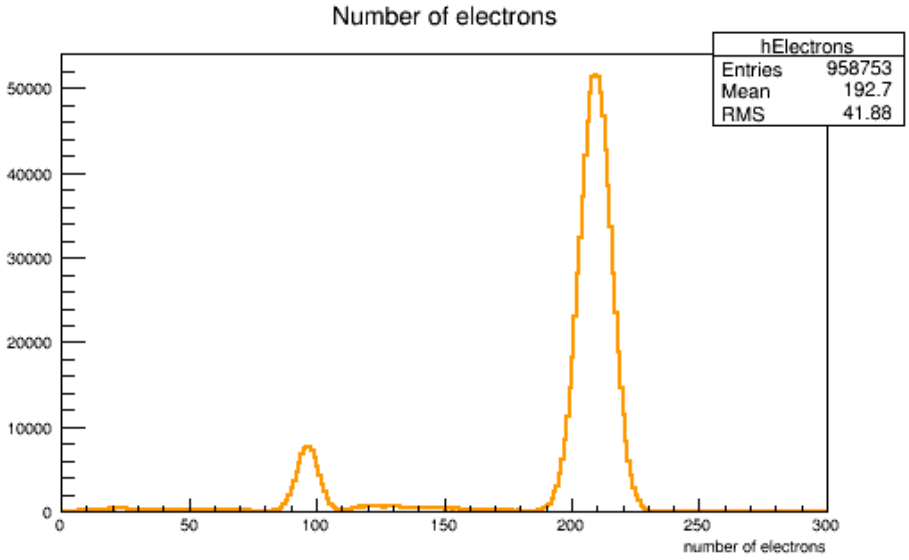

Figure 4.3: The number of primaries generated from an ^{55}Fe source. The small peak is the argon escape peak.

that have a binding energy of 3206 eV [17], is excited to the continuum. If such an electron absorbs a 5.9 keV photon it will be released into the gas with a correspondingly lower energy, which will result in fewer primaries being generated. This was also tested by performing the same simulations at lower photon energies. As expected the spectrum consisted of only one peak when the photon energy was below 3.2 keV. Simulations were also carried out for mixtures of argon and carbon dioxide in the ratios 76/24 and 82/18. The number of primaries for these mixtures were 212.1 ± 6.31 and 214.7 ± 6.34 for the full energy peak and 97.91 ± 4.57 and 99.27 ± 4.58 for the argon escape peak, respectively.

4.5 Gain simulation

The gain of the GEM is simulated by releasing an electron at a position near the top of the drift volume. The electron is then transported through the detector creating an avalanche on its way. The number of electrons that reach the readout plane is then counted to give the gain.

The simulations were done using the standard configuration of the detector with a filling gas of argon and carbon dioxide in the mixing ratios used in the measurements. Voltage was applied corresponding to the total voltage 3900 V, 3950 V, and 4000 V shown in table 3.1. The probability for the Penning effect to occur, given by the Penning coefficient, was set to 0.57, 0.56, and 0.53 for the different gas mixtures, as reported in [4]. The result from the simulations is shown in figure 4.4. These simulations were done with one starting electron, corresponding to the Poisson distribution for the avalanches for $N = 1$ in figure 2.1. Such an avalanche for a gas mixture of Ar/CO_2 in the ratio 70/30 is seen in figure 4.5. The orange lines are the electron tracks and the grey lines are the GEM foils. The total number of tracks created in the avalanche was 4095. The spread of the electron cloud when it reaches the readout plane at -0.4 cm is $\sim$1 mm.

For an incoming particle there is a spread in the number of primaries generated and the estimated error for the one electron case does not take this in account. To get a further estimate of the error, and the intrinsic resolution of the detector, an electron was also released with a starting energy of 5.9 keV, corresponding to photo absorption of an incoming gamma ray from ^{55}Fe. Such an electron will generate delta electrons through ionization of the gas. All electrons created are transported through the detector and the number of electrons that reach the readout plane is counted, in the same way as for the one electron case. Since the number of starting electrons is now around 200 (figure 4.3) the avalanche size will follow a Gaussian distribution. The result for 4000 V with Ar/CO_2 70/30 is shown in figure 4.4d. The data is fitted with a Gaussian with mean 1041 and standard deviation of 72.36. The corresponding FWHM resolution is 16 %.

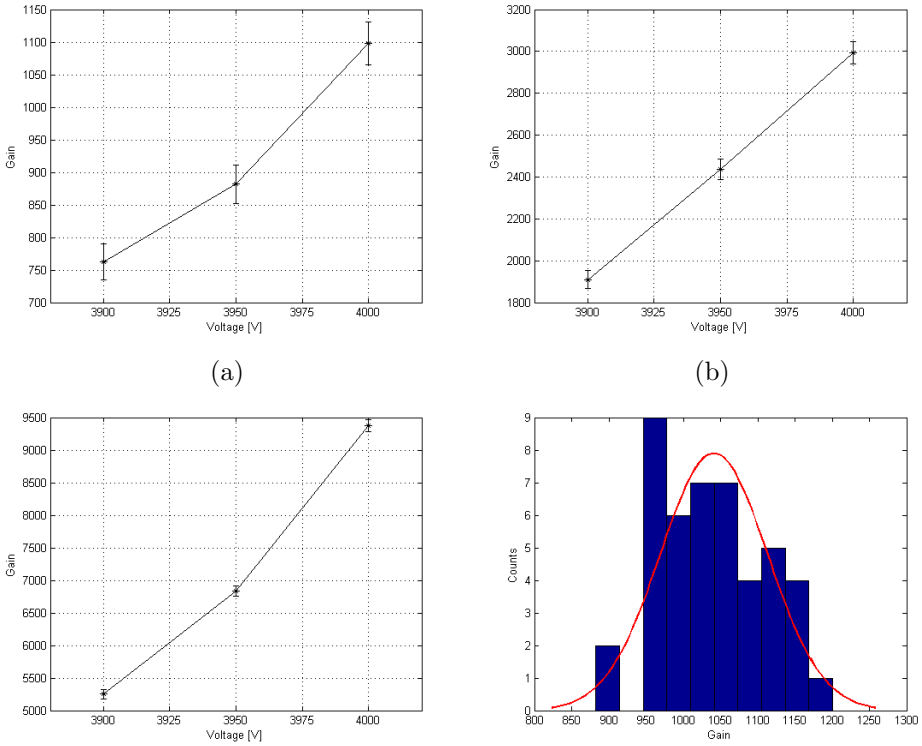

Figure 4.4: a)-c) Gain for of a triple GEM in the standard configuration for different gas mixtures(70/30, 76/24, 82/18). The simulations was done with a single starting electron. d) Gain for an electron with an energy of 5.9 keV. The resulting distribution is fitted with a Gaussian.

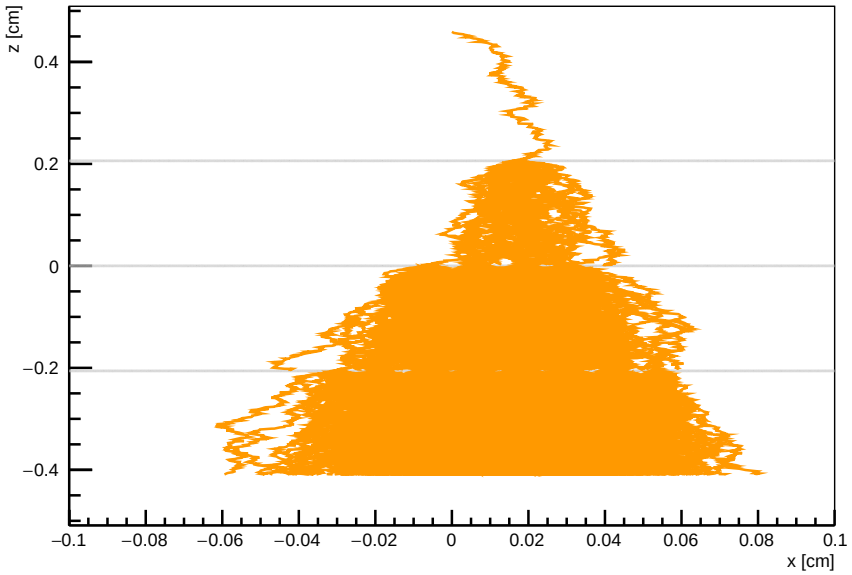

Figure 4.5: An avalanche of a single electron in Ar/CO_2 70/30. The voltage across the detector was 3800 V. The electron tracks are shown in orange and the GEM foils in grey.

4.6 Signal simulation

In Garfield++ it is possible to simulate the signal that is induced from the electrons and the ions given the proper weighting potential maps. The induced current from a charge on a given electrode j can be calculated with the Shockley-Ramo theorem, equation 4.2.

$$i_j = -q\vec{v} \cdot \vec{F}_j \tag{4.2}$$

where i_j is the induced current on electrode j, q the charge of the particle, $\vec{v}$ the velocity of the particle, and $\vec{F}_j$ the weighting field for the j:th electrode. The weighting potential is calculated by setting the potential on conductor j to one and zero on all other potentials and solving for the potential. The weighting field is then calculated by $\vec{F}_j = -\nabla V$ [14]. The weighting potential is calculated with the same program that calculated the electric fields by changing the boundary conditions. A calculated signal for a triple GEM is shown in figure 4.6. The signal was calculated with a gas mixture of Ar/CO_2 82/18. The voltage across the detector corresponds to the total voltage of 4000 V shown in table 3.1. The drift time for the electrons to reach the readout plane after a photon interacts in the detector volume was for this case ∼80 ns, and the total charge was collected within ∼40 ns.

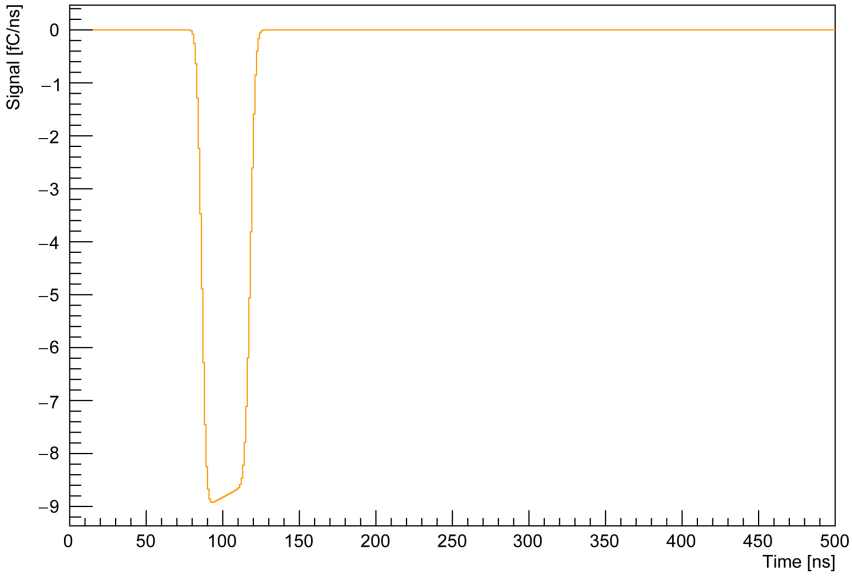

Figure 4.6: The signal induced from in a triple GEM from a 5.9 keV photon. The gas mixture in the detector was Ar/CO_2 82/18, and the voltage was 3800 V.

As mentioned in section 3.3.5 the Bode diagrams were measured for the amplification stages used in the measurements. The plan is to extend those measurements for other types of preamplifiers intended for use with the detector in the future. Those studies will also include using several different input pulses, in order to have a larger set of pulses. That work is ongoing but beyond the scope of the current work.

Chapter 5

Results and Conclusions

The use of GEM foils for electron multiplication has been tested by assembly in the small prototype detector. Working with GEM foils requires easy access to a clean room, which makes assembling and dissembling the detector, in different configurations, time consuming. It is therefore interesting to see how robust GEM foils would be in an experimental environment, that would require regular changes in the setup. Experience shows that in addition to having access to a clean room, the practical work for changing of the foils took up to two hours. The main reason for working in a clean room was to prevent dust deposition on the foils. During this work it was found that small amounts of dust can be burned of under controlled environments. This is done by applying a voltage of ∼600 V across the foil while monitoring the current. If during this process the rate of discharges in the foils decreases and the leakage current stabilizes at ∼10 nA the foil will be functional. For that procedure it is important that the voltage supply has a current limitation of a few μA. Nevertheless, the foils can easily be destroyed if handled carelessly. Due the relatively long time it takes to change the setup in a GEM detector it is important to be able to test different configurations through simulations.

5.1 Detector characteristics

After assembly of the detector in the configuration described in section 3.1, rate curves were measured for three different gas mixtures of Ar/CO_2 in the ratios 70/30, 76/24, and 82/18. It was found that the charge collection starts in the region around 3700 V and reaches the plateau at a few hundred volts higher for this configuration, but depends on the amount of quencher in the gas. The charge collection begins at lower voltages for the mixtures with less quencher, namely at 3900 V, 3650 V, and 3550 V, respectively. The current on the readout plane was measured in order to calculate the gain, which also depends on the number of primaries. The gain at 4000 V

for the different gas mixtures were 1500, 4500, and 15000. From section 2.4 it is clear that an decreasing amount of quencher in the gas mixture will increase the gain. Since more energy is used to create electron-ion pairs. This can also be seen in figure 3.6, where the gain for a specific voltage is higher with less carbon dioxide in the mixture. Similarly this is also seen in the rate curves where the plateau is reached with lower voltage for the mixtures with less carbon dioxide. All tests were done with a ^{55}Fe source to simulate a minimum ionizing particle. Since the intended use is to detect charged particles the best option is the mixture with the largest amount of quencher, because the particle will create more primaries which does not require as high gain and gives a safer operational condition with respect to discharges.

The simulations resulted in a gain of 1100, 3000, and 9500 at 4000 V in the different gas mixtures, respectively. This follows the same trend as the measured gain, increasing with a decreasing fraction of quencher. It also increases with increasing potential difference across the detector. The simulated gain is not exact but gives a good description of the trend of the detector and comparison between different gas mixtures. The agreement is best for the mixture with the largest amount of quencher. This suggest that Garfield++ can used to test different configuration for the final design of the detector. The good agreement also means that it can be used to simulate other aspects than the gain.

To calculate the gain from the measurement the number of primaries is needed. The cross section for the different interaction processes with the gas is rather well known, which makes it a viable option to simulation the number of primaries. The result was 209.5$\pm$6.31, 212.1$\pm$6.31, and 214.7$\pm$6.34 primaries for the three different gas mixtures. The error from these simulations was propagated into the error of the gain, and was found to give a negligible contribution.

The avalanche size of a full energy event was also simulated by sending in an electron with an energy of 5.9 keV, this more realistic simulation resulted in a spread of 6.95 % compared to a spread of 3.02 % for an avalanche starting from a single electron. It's worth noticing that this simulation took three days compared to below one day for the single electron case.

The simulated signal shows a rapid rise and fall time. It has a duration of around 30-40 ns. It also shows that it takes $\sim$ 85 ns for the electron cloud to reach the bottom of the third foil and start inducing the signals. The times are dependent on the type of gas used and on the field strength in the drift, induction, and, transfer regions.

In figure 4.5 the electron cloud can be seen. The spread is around 1 mm, this influence the size of the pads/strips needed for good resolution on the readout board.

For further studies of the measured pulse shapes, the Bode diagrams were measured for the amplifiers used here. The next step is to measure

Bode diagrams for several differnt amplifiers and also simulate more pulses.

5.1.1 Charge up

For long duration measurements there can be charge deposition on the insides of the holes in the foils, which leads to changes in the gain of the detector (see section 2.5.4). Figure 3.7b shows that it take some time for the foils to charge up. In this test the detector reaches a stable gain plateau after approximately 5.5 hours, however it is possible to reach the gain plateau faster using a higher intensity source. The change in relative gain is consistent with reported values in [11].

5.1.2 Leakage test

The leakage test, as seen in figure 3.7a, showed that there is no change in the gain of the detector for the first 200 seconds of the test. This is probably because there is still argon gas in the hoses that are connected to the detector and it takes a while before the gas is removed and only carbon dioxide that is flowing through the pipes. Then there is a rapid decrease in the gain, where it goes to zero over a period of 200 s. As expected, the test suggests that a leak can go unnoticed for a time depending on the size of the gas volume and flow.

Chapter 6

Summary and Outlook

GEM foils have been tested for the electron multiplication stage for a tracking detector for nuclear physics experiments. Measurements of rate curves and gain have been performed. Tests of foil charge up and the response to a gas leak have been carried out. Results have been compared to simulations in Garfield++. The conclusion is that the simulations agree with measurements within expectation.

To further investigate the detector for use as an active target there are several additional tests that should be performed. This includes building and testing a field cage for detection of ions, designing and testing a dedicated readout plane, setting up and testing the gas system for different gases and pressures intended for the experiments. Counting rate tests need also to be performed in order to investigate compatibility with intended experiments.

Bibliography

[1] Actar. Actar an active target detector for study of extremley exotic nuclei. *Ganil*, 2009.

[2] M. Norrby. *Alpha-Cluster Structures in Medium Light Nuclei.* PhD thesis, Åbo Akademi University, 2011.

[3] F. Sauli. *Gaseous Radiation Detectors: Fundamentals and Applications.* Cambridge University Press, 2014.

[4] Ö. Sahin, I. Tapan, E.N. Özmutlu, and R. Veenhof. Penning transfer in argon-based gas mixtures. *Journal of Instrumentation*, 2010.

[5] S. Bachmann, A. Bressan, L. Ropelewski, F. Sauli, A. Sharma, and D. Mörmann. Charge amplification and transfer processes in the gas electron multiplier. *Nuclear Instruments and Methods in Physics Research A*, 438:376–408, 1999.

[6] F. Sauli. The gas electron multiplier (gem): Operating principles and applications. *Nuclear Instruments and Methods in Physics Research A*, 805:2–24, 2016.

[7] F. Sauli. Gem: A new concept for electron amplification in gas detectors. *Nuclear Instruments and Methods in Physics Research A*, 386:531–534, 1997.

[8] S. Bachmann, A. Bressan, M. Capeáns, M. Deutel, S. Kappler, B. Ketzer, A. Polouektov, L. Ropelewski, F. Sauli, E. Schulte, L. Shekhtman, and A. Sokolov. Discharge studies and prevention in the gas electron multiplier (gem). *Nuclear Instruments and Methods in Physics Research A*, 479:294–308, 2002.

[9] M. Ball, K. Eckstein, and T. Gunji. Ion backflow studies for the alice tpc upgrade with gems. *3rd International Conference On Micro Pattern Gaseous Detectors*, 2013.

[10] J. Benlloch, A. Bressan, M. Capéans, M. Gruwé, M. Hoch, J.C. Labbé, A. Placci, L. Ropelewski, and F. Sauli. Further developments and beam

test of the gas electron multiplier (gem). *Nuclear Instruments and Methods in Physics Research A*, 419:410–417, 1998.

[11] F. Simon, B. Azmoun, U. Becker, L. Burns, D. Crary, K. Kearney, G. Keeler, R. Majka, K. Paton, G. Saini, N. Smirnov, B. Surrow, and C. Woody. Development of tracking detectors with industrially produced gem foils. *arXiv:0707.2543v2*, 2007.

[12] F. Sauli. Imaging with the gas electron multiplier. *Nuclear Instruments and Methods in Physics Research A*, 580:971–973, 2007.

[13] CSC-IT Center for Science LTD. Elmer. `https://www.csc.fi/web/elmer/elmer`. Acessed: 2015-11-17.

[14] `http://garfieldpp.web.cern.ch/garfieldpp/`. Acessed: 2015-11-27.

[15] C. Geuzaine and J.-F. Remacle. Gmsh: a three-dimensional finite element mesh generator with built-in pre- and post-processing facilities. *International Journal for Numerical Methods in Engineering*, 79(11):1309–1331, 2009.

[16] N. Ottosen and H. Petersson. *Introduction to the finite element method*. Prentice Hall, 1992.

[17] `http://xdb.lbl.gov/Section1/Table_1-1.pdf`. Acessed: 2015-12-08.